Thermal theory for heterogeneously architected structure: Fundamentals and application

Liujun Xu, Shuai Yang, and Jiping Huang*

Department of Physics, State Key Laboratory of Surface Physics, and Key Laboratory of Micro and Nano Photonic Structures (MOE), Fudan University, Shanghai 200433, China

(Received 14 September 2018; published 26 November 2018)

Architected structures have aroused widespread research interest because they possess unique properties in mechanics. However, a fundamental theory describing their thermal properties has not been established. Here, we present a theoretical framework in thermotics to predict thermal properties of architected structures. Then, by experiment and simulation, we show its applications in the field of heat management. By assembling two radically different materials, we design two types of Janus structures. The different rotation degrees of the Janus structures can flexibly control the switch between different functions, such as from partial concentration to uniform concentration and from rotation to concentration. These functions are realized in a structure made of a heterogeneous core plus a homogeneous shell, which is in contrast to the existing structures made of a homogeneous core plus a heterogeneous shell designed according to the theory of transformation thermotics. This work lays a theoretical foundation in thermotics for further research on heterogeneously architected structures, and it proposes the concept of thermal Janus structures for flexible heat control, which may open an avenue for intelligent thermal metamaterials.

DOI: 10.1103/PhysRevE.98.052128

I. INTRODUCTION

Heat manipulation is of growing significance due to the universality of heat energy. Fortunately, with delicate design of architected structures, many unique thermal phenomena have been realized, which include cloaking or camouflage [1–15], concentration [4,9,16,17], rotation [4,18], transparency [19], and their combinations [20–25]. These functions are mostly based on the structure of a coated core, which is generally featured by a homogeneous core and a heterogeneous (architected) shell according to the theory of transformation thermotics [1–3]. Even so, heterogeneously architected structures have aroused less attention in thermotics than in mechanics (e.g., see Ref. [26] and references therein). This situation mainly results from the lack of enough fundamental thermal theories for handling heterogeneously architected structures.

As a meaningful attempt, here we introduce the structure of a coated core, which is, however, composed of a heterogeneously architected core and a homogeneous shell. A theoretical framework will be established to predict the effective thermal response of the coated core.

In addition, another challenge is to realize multifunctions in a single field. Compared with multifunctions in multifields [20–24], there is only one adjustable parameter in a single field (such as thermal conductivity in the single thermal field), so the realization of multifunctions in a single field becomes relatively more difficult. Although Shen *et al.* [25] have realized a type of cloak-concentrator in thermotics by tailoring the temperature-dependent effect of thermal conductivities, different mechanisms for multifunctions still remain to be investigated.

To overcome this challenge, here we further propose a concept of a thermal Janus core on the basis of the aforementioned theoretical framework, which can be seen as a typical kind of heterogeneously architected core. Generally speaking, such a Janus core is composed of two radically different materials, and has been widely studied in soft matter (e.g., see Refs. [27–29]). Then we experimentally fabricate two samples to realize the flexible control of isotherm concentration by rotating the core. We further propose another concept of a generalized thermal Janus core, which is also composed of two radically different materials, but with more flexible structures. As a result, the switch between thermal rotation and concentration can be achieved by rotating the core.

II. THEORY

Let us start by investigating the effective thermal conductivity of a two-dimensional coated core with circular shape; see Fig. 1(a). The thermal property of the core is represented by a heterogeneous, anisotropic, and diagonal thermal conductivity tensor $\overleftrightarrow{\kappa}_c(x, y)$,

$$\overleftrightarrow{\kappa}_c(x, y) = \begin{bmatrix} \kappa_{xx}(x, y) & 0 \\ 0 & \kappa_{yy}(x, y) \end{bmatrix}. \tag{1}$$

We then write down the boundary condition [heat flux $\boldsymbol{J}_b(x, y)$] on Boundary I [see Fig. 1(b)] in Cartesian coordinates according to Fourier's law,

$$\begin{aligned} \boldsymbol{J}_b(x, y) &= \begin{bmatrix} J_x(x, y) \\ J_y(x, y) \end{bmatrix} = -\overleftrightarrow{\kappa}_c(x, y)\nabla T_b(x, y) \\ &= -\begin{bmatrix} \kappa_{xx}(x, y)\partial T_b(x, y)/\partial x \\ \kappa_{yy}(x, y)\partial T_b(x, y)/\partial y \end{bmatrix}, \end{aligned} \tag{2}$$

*jphuang@fudan.edu.cn

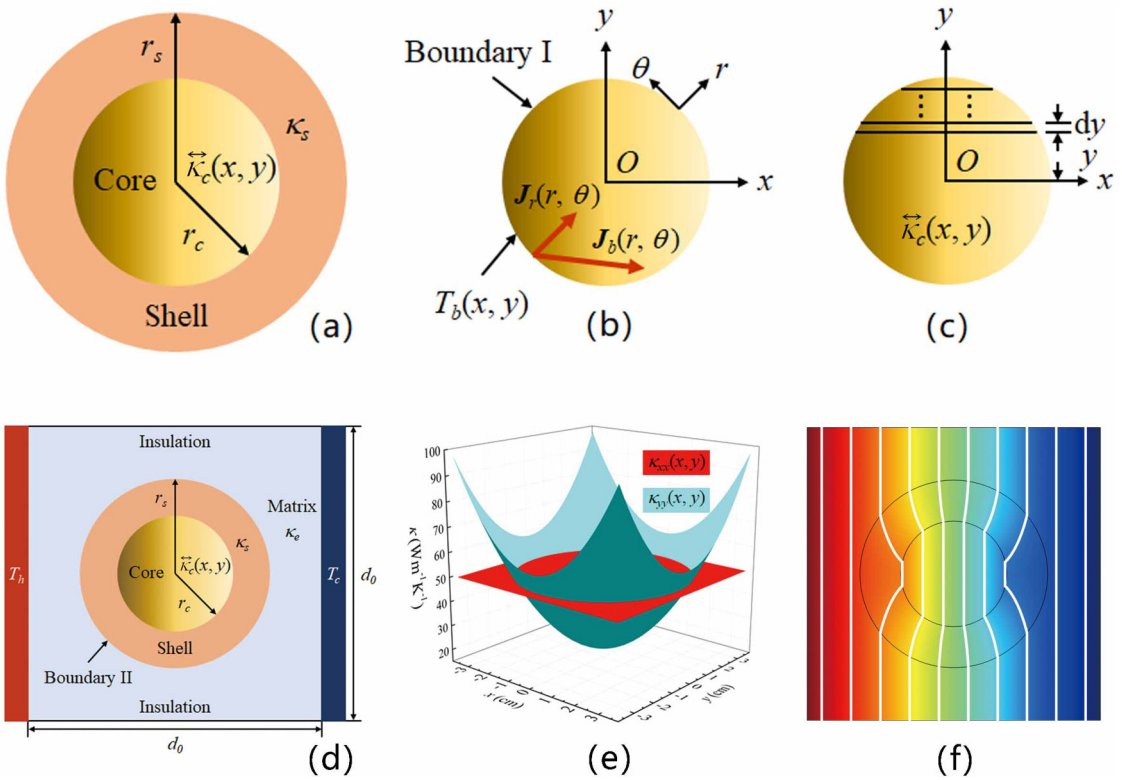

FIG. 1. Schematic diagrams (a)–(c) and simulation settings (d) and (e) of a coated core: (a) structures and parameters, (b) boundary conditions (heat flux and temperature), and (c) calculating method; (d) simulation box and (e) thermal conductivities of the core. (f) shows the simulation result with $\overleftrightarrow{\kappa}_c = \mathrm{diag}[50,\ 20 + 30000(x^2 + y^2)]$, $\kappa_s = 400$, and $\kappa_e = 242\,\mathrm{Wm^{-1}K^{-1}}$. Parameters: $T_h = 313\,\mathrm{K}$, $T_c = 273\,\mathrm{K}$, $d_0 = 20\,\mathrm{cm}$, $r_c = 3.6\,\mathrm{cm}$, and $r_s = 6.4\,\mathrm{cm}$. White lines represent isotherms.

where $T_b(x, y)$ is the temperature distribution on Boundary I [see Fig. 1(b)]. We rewrite the heat flux $\boldsymbol{J}_b(x, y)$ in polar coordinates for the convenience of discussion,

$$\boldsymbol{J}_b(r,\theta) = \begin{bmatrix} J_r(r,\theta) \\ J_\theta(r,\theta) \end{bmatrix} = \begin{bmatrix} J_x(x,y)\cos\theta + J_y(x,y)\sin\theta \\ -J_x(x,y)\sin\theta + J_y(x,y)\cos\theta \end{bmatrix}, \tag{3}$$

where $x = r\cos\theta$, $y = r\sin\theta$.

Now we pay attention to the radial component $J_r(r, \theta)$ [see Fig. 1(b)], because heat flux is always conservative along the radial direction of Boundary I,

$$\begin{aligned} J_r(r,\theta) = &-\kappa_{xx}(x,y)\cos\theta\,\partial T_b(x,y)/\partial x \\ &-\kappa_{yy}(x,y)\sin\theta\,\partial T_b(x,y)/\partial y. \end{aligned} \tag{4}$$

For further discussion, we have to make an approximation for the boundary condition [temperature $T_b(x, y)$]. Namely, when the direction of external thermal field is along the x axis and $\kappa_{xx}(x, y)$ is a constant, the temperature distribution on Boundary I is uniform,

$$T_b(x, y) = Ax + B, \tag{5}$$

where A and B are two constants. We suppose that Eq. (5) holds approximately when $\kappa_{xx}(x, y)$ experiences a small variation. Therefore, the radial component of heat flux Eq. (4) can be simplified to

$$J_r(r,\theta) = -\kappa_{xx}(x,y)A\cos\theta. \tag{6}$$

The most important feature of Eq. (6) is that $J_r(r, \theta)$ is independent of $\kappa_{yy}(x, y)$, which means that the effective thermal conductivity of the coated core is independent of $\kappa_{yy}(x, y)$. In other words, we only need to calculate the effective thermal conductivity of $\kappa_{xx}(x, y)$ (denoted by scalar κ_c), and then the effective thermal conductivity of the coated core can be obtained. Therefore, as long as the variation of $\kappa_{xx}(x, y)$ is small enough, Eq. (5) is rational and contributing.

Now we are in a position to calculate the effective thermal conductivity of $\kappa_{xx}(x, y)$, namely κ_c. The concrete approximation method is as follows.

We first separate the core into strips whose width dy is small enough; see Fig. 1(c). Then we calculate the effective thermal conductivity of each strip $\kappa_{xx}(y)$ through series connection,

$$\kappa_{xx}(y) = \frac{2\sqrt{r_c^2 - y^2}}{\int_{-\sqrt{r_c^2-y^2}}^{\sqrt{r_c^2-y^2}} \frac{dx}{\kappa_{xx}(x,y)}}, \tag{7}$$

where r_c is the radius of the core.

We further calculate the effective thermal conductivity of these strips through parallel connection,

$$\kappa_c = \int_{-r_c}^{r_c} \frac{2\kappa_{xx}(y)\sqrt{r_c^2 - y^2}\,dy}{\pi r_c^2}. \tag{8}$$

We finally calculate the effective thermal conductivity of the coated core κ_e through the single-particle effective

medium theory, namely Eq. (11) in Ref. [30],

$$\kappa_e = \kappa_s \frac{\kappa_c + \kappa_s + (\kappa_c - \kappa_s)p}{\kappa_c + \kappa_s - (\kappa_c - \kappa_s)p}, \tag{9}$$

where κ_s is the thermal conductivity of the shell and $p = (r_c/r_s)^2$ is the area fraction of the core.

The final results, Eqs. (7)–(9), are independent of $\kappa_{yy}(x, y)$ under the approximation condition of Eq. (5). We mention that the influence of the conductivity variation on the accuracy of Eqs. (7)–(9) is analyzed in Sec. III via finite-element simulations.

Similarly, we can calculate the effective thermal conductivity of a three-dimensional coated core with spherical shape, as shown in the Appendix.

III. SIMULATION

We simulate the two-dimensional coated core [see Fig. 1(d)] to observe the performance of Eqs. (7)–(9). For arbitrary $\kappa_{xx}(x, y)$, well-defined (or strict) effective thermal conductivity of a coated core probably does not exist. Therefore, we define a relative error Δ to indirectly examine the performance of Eqs. (7)–(9) on predicting the effective thermal conductivity,

$$\Delta = \frac{\oint_\Sigma |\nabla T - \nabla T_0| dl}{|\nabla T_0| \oint_\Sigma dl}, \tag{10}$$

where ∇T_0 is the external thermal field, $|\nabla T_0| = (T_h - T_c)/d_0$, and the integrate boundary Σ is the outer periphery of the coated core (denoted by Boundary II); see Fig. 1(d). Clearly, better performance of Eqs. (7)–(9) corresponds to less influence of the coated core on the matrix, which is represented by a smaller value of Δ. For our purpose, we calculate Eq. (10) by using a finite-element simulation based on the commercial software COMSOL MULTIPHYSICS [31].

We have mentioned that when $\kappa_{xx}(x, y)$ is a constant, Eq. (5) is strictly satisfied and κ_e is independent of $\kappa_{yy}(x, y)$. To validate the statement, we set $\kappa_{xx}(x, y) = 50\,\mathrm{Wm^{-1}K^{-1}}$ and arbitrary $\kappa_{yy}(x, y) = 20 + 30000(x^2 + y^2)\,\mathrm{Wm^{-1}K^{-1}}$; see Fig. 1(e). The thermal conductivity of the shell κ_s is set to be $400\,\mathrm{Wm^{-1}K^{-1}}$, and the effective thermal conductivity of the coated core is calculated from Eqs. (7)–(9). We find that the temperature gradient in the core is uniform—see Fig. 1(f)—and obtain $\Delta = 0$ according to Eq. (10). The results indicate that when $\kappa_{xx}(x, y)$ is a constant, Eqs. (7)–(9) can be reduced to account for the known case of uniform thermal conductivities.

Now we discuss a position-dependent $\kappa_{xx}(x, y)$. Our theory [Eqs. (7)–(9)] does not consider the effect of $\kappa_{yy}(x, y)$, so we set $\kappa_{yy}(x, y) = \kappa_{xx}(x, y)$ without loss of generality. We choose two typical functions: $F(w) = 20 + |100w|^C$ and $G(w) = 20 + 60/(1 + e^{-100Dw})$, which are respectively even-symmetric and odd-symmetric; see Figs. 2(a) and 2(d). To distinguish the contribution, we respectively set $\kappa_{xx}(x, y) = F(x)$, $\kappa_{xx}(x, y) = F(y)$, $\kappa_{xx}(x, y) = G(x)$, and $\kappa_{xx}(x, y) = G(y)$. The effective thermal conductivities and relative errors are respectively shown in Figs. 2(b), 2(e) and Figs. 2(c), 2(f). The maximum relative error is below 1.9%, which shows the ability of our theory to predict the

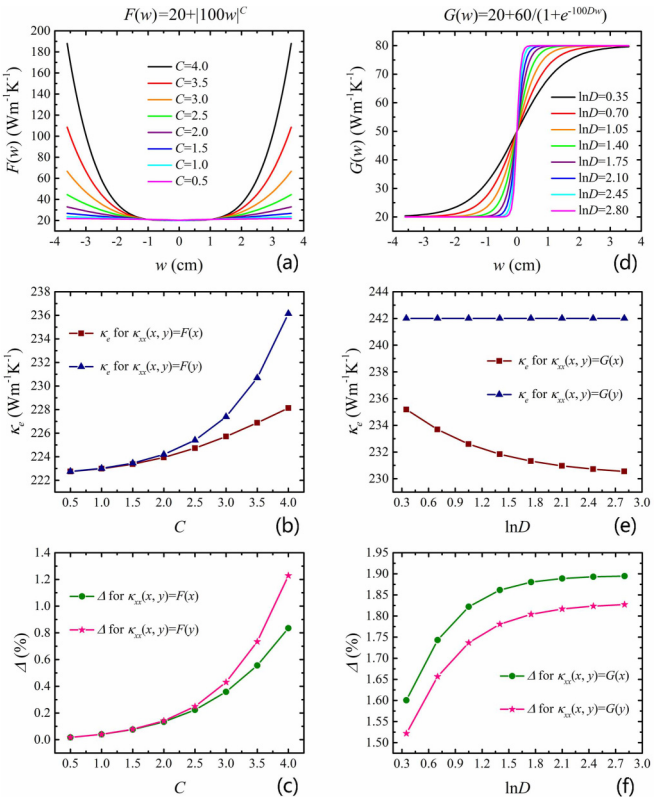

FIG. 2. Simulation results of a coated core. (a) and (d) are two typical functions which will be set as the thermal conductivities of the core. (b) and (e) are the predicted effective thermal conductivities of the coated core with Eqs. (7)–(9). (c) and (f) are the relative errors of the predicted thermal conductivities with Eq. (10). Other simulation settings are same as those for Fig. 2(d).

effective thermal conductivities. In $F(w)$ and $G(w)$, C can reflect the variation amplitude, and ln D can reflect the variation speed. Comparing Figs. 2(c) and 2(f), we find that the relative errors increase as the variation amplitude (C) and variation speed (ln D) increase. In addition, the relative errors of even-symmetric distribution [$F(w)$] of thermal conductivities are smaller than those of the odd-symmetric distribution [$G(w)$].

IV. APPLICATION: EXPERIMENT AND SIMULATION

A. Thermal Janus core

The above theories and simulations pave the way to propose a concept of a thermal Janus core which is composed of two radically different materials (material A and material B); see Fig. 3(a). Here we apply such a thermal Janus core to realize the manipulation of isotherm concentration; see Figs. 3(b) and 3(c). We can observe the partial concentration of the isotherms in Fig. 3(b). The isotherms become concentrated in the left part of the core, while they are sparse in the right. Then we anticlockwise rotate the thermal Janus core by 90°, and we observe the uniform concentration of the isotherms in Fig. 3(c). The concrete concentration ratio is shown in Fig. 3(j). To ensure that the rotation will not disturb the external field, the thermal conductivity of the core is required to satisfy

$$(\kappa_c)_0 = (\kappa_c)_{90}, \tag{11}$$

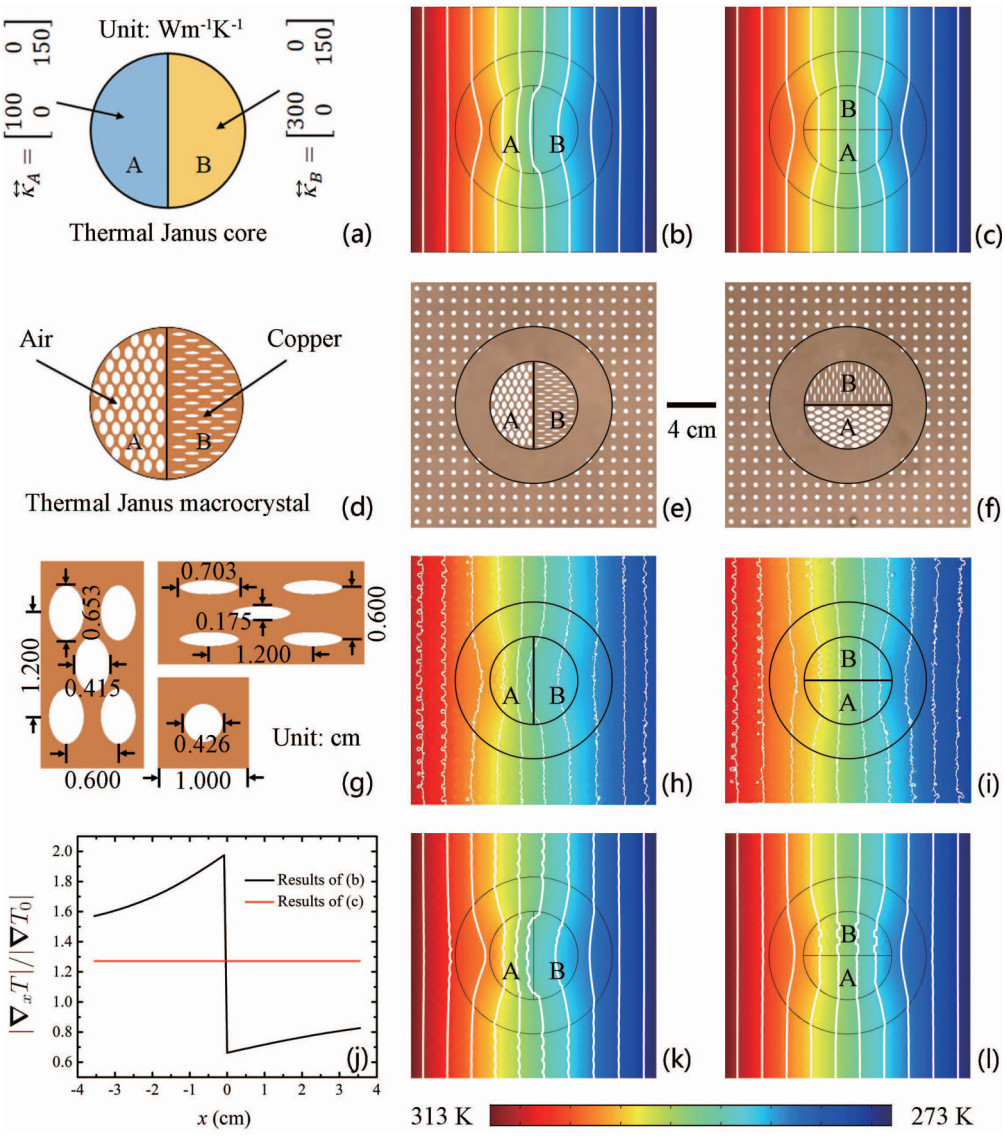

FIG. 3. Thermal Janus core. (a) and (d) are the ideal thermal Janus core and practical thermal Janus macrocrystal. (b) is the simulated result of partial concentration (left part of the core). (c) shows the simulated results of uniform concentration where the core is anticlockwise rotated by 90°. (e) and (f) are two fabricated samples whose measured and simulated results are respectively shown in (h),(i) and (k),(l). The detailed parameters are displayed in (g). (j) shows the concentration ratio in the core along the x axis (where $y = 0$). Parameters: $\overleftrightarrow{\kappa}_A = \mathrm{diag}[100,\ 150]\,\mathrm{Wm^{-1}K^{-1}}$, $\overleftrightarrow{\kappa}_B = \mathrm{diag}[300,\ 150]\,\mathrm{Wm^{-1}K^{-1}}$; copper: $400\,\mathrm{Wm^{-1}K^{-1}}$; air: $0.026\,\mathrm{Wm^{-1}K^{-1}}$, and other parameters are same as those for Fig. 2(d).

where the subscripts 0 and 90 respectively represent the anticlockwise rotation angle of the core, and they can be calculated from Eqs. (7)–(9). When calculating $(\kappa_c)_{90}$, the $\kappa_{yy}(x, y)$ in Eq. (1) actually works, and hence $\kappa_{xx}(x, y)$ in Eqs. (7)–(9) should be replaced by $\kappa_{yy}(x, y)$.

In the mean time, we also conducted experiments for demonstration. We drilled different holes in a copper plate to design practical structures of the core, and fabricates two samples with laser engraving; see Figs. 3(d)–3(f). Detailed parameters of the two experimental samples were designed according to the periodic-particle effective medium theory, namely Eq. (4) in Ref. [32], and are shown in Fig. 3(g). We used water baths to act as hot or cold sources, and an infrared camera Flir E60 to detect the thermal profile. The measurements were conducted at standard atmosphere pressure and room temperature. The measured and simulated results based on the two samples are respectively shown in Figs. 3(h), 3(i) and Figs. 3(k), 3(l). Clearly, there is good agreement with our theory.

Then we rotate the core by 22.5°, 45°, and 67.5° to observe the switch progress from partial concentration to uniform concentration: Figs. 4(a)–4(c) for anticlockwise rotation, Figs. 4(d) and 4(f) for clockwise rotation. Owing to Eq. (11), the external field is not disturbed as expected.

B. Generalized thermal Janus core

We further propose another concept of a generalized thermal Janus core which is also composed of two radically different materials (material A and material B), but with more flexible structures; see Fig. 5(a). Here we apply such a generalized

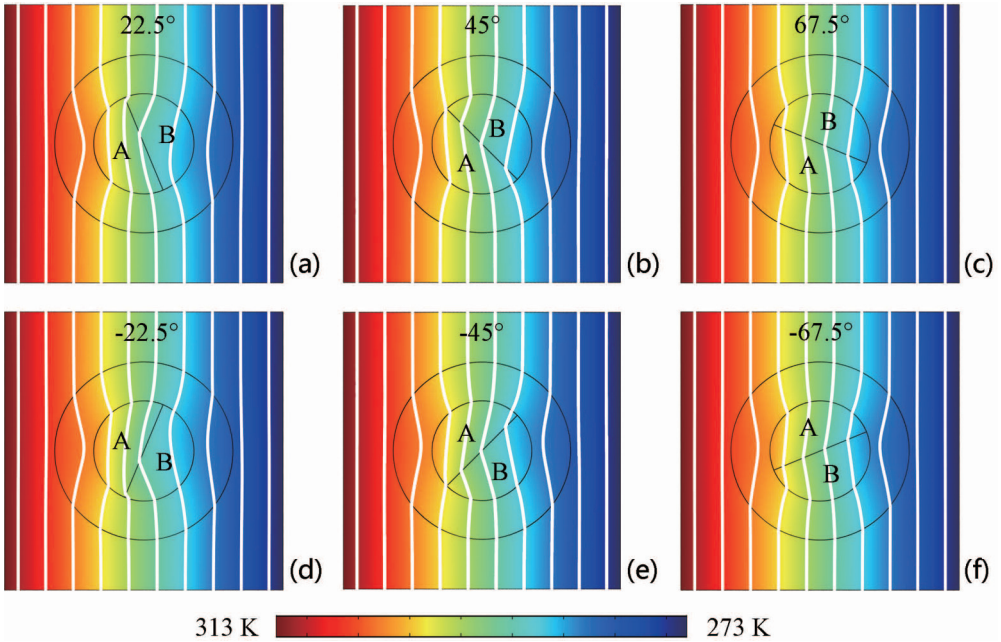

FIG. 4. Simulated results for anticlockwise (a)–(c) and clockwise (d)–(f) rotations of the core by 22.5°, 45°, and 67.5°. Other parameters are same as those for Fig. 3(b).

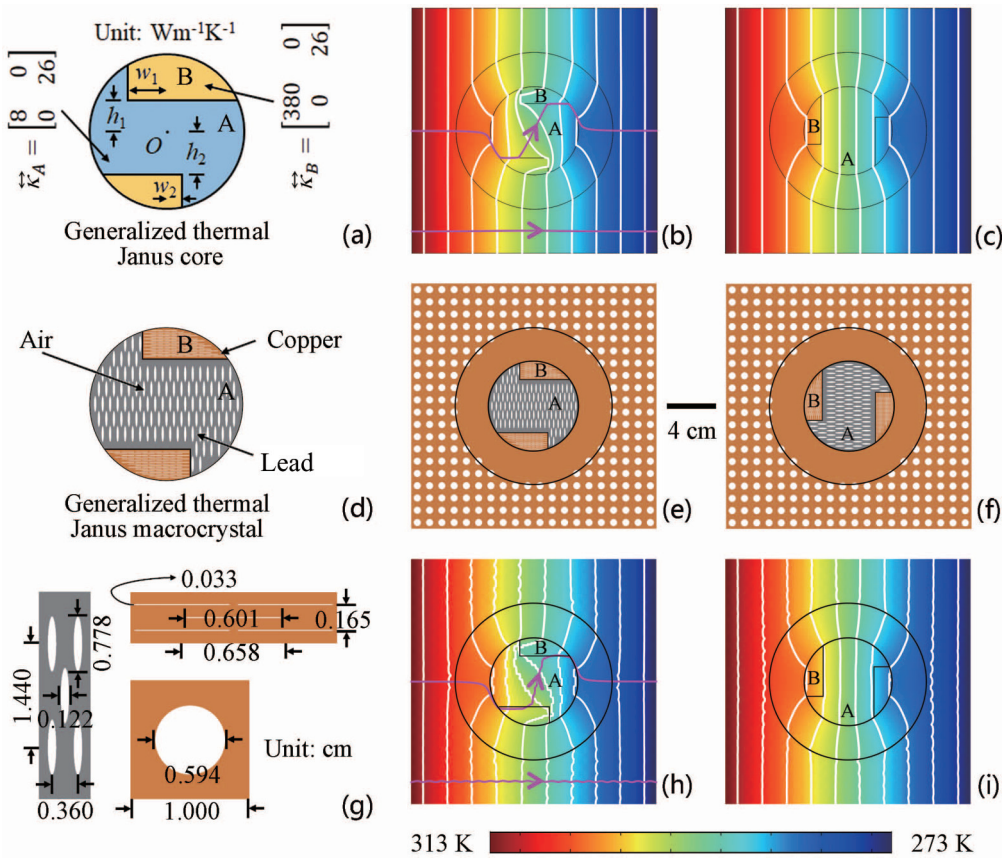

FIG. 5. Generalized thermal Janus core. Purple lines in (b), (c), (h), and (i) represent the flow of heat. (a) and (d) show the ideal generalized thermal Janus core and practical generalized thermal Janus macrocrystal, respectively. (b) is the simulated result of heat flux rotation. (c) is the simulated results of concentration where the core is anticlockwise rotated by 90°. (e) and (f) are two designed samples whose simulated results are shown in (h) and (i). The detailed parameters are displayed in (g). Parameters: $\overleftrightarrow{\kappa}_A = \mathrm{diag}[8,\ 26]\,\mathrm{Wm^{-1}K^{-1}}$, $\overleftrightarrow{\kappa}_B = \mathrm{diag}[380,\ 26]\,\mathrm{Wm^{-1}K^{-1}}$; lead: $35\,\mathrm{Wm^{-1}K^{-1}}$, $h_1 = h_2 = 2.12\,\mathrm{cm}$, $w_1 = w_2 = 1.11\,\mathrm{cm}$, and other parameters are same as those for Fig. 2(d).

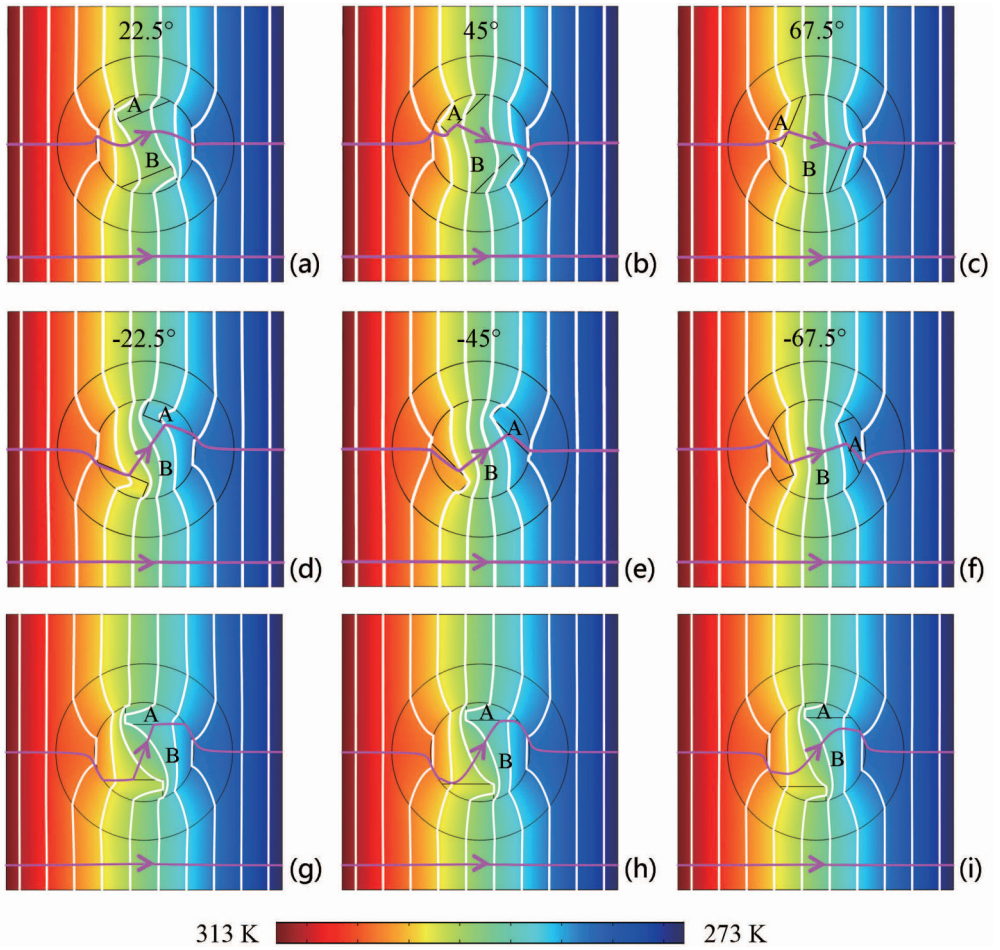

FIG. 6. Simulated results for other parameters. Anticlockwise (a)–(c) and clockwise (d)–(f) rotations of the core by 22.5°, 45°, 67.5°. (g)–(i) show changing parameters h_1, h_2, w_1, and w_2. Parameters: $h_1 = h_2 = 2.50$ cm and $w_1 = w_2 = 0.75$ cm for (g), $h_1 = h_2 = 2.31$ cm and $w_1 = w_2 = 0.99$ cm for (h), $h_1 = h_2 = 2.01$ cm and $w_1 = w_2 = 1.35$ cm for (i), and other parameters are same as those for Fig. 5(b).

thermal Janus core to realize the switch between concentration and rotation; see Figs. 5(b) and 5(c). Figure 5(b) shows that the heat flux in the core has a rotation of about 62°, when compared with that in the matrix. Then we anticlockwise rotate the generalized thermal Janus core by 90°, and we can observe the switch from rotation to concentration in Fig. 5(c). Incidentally, when designing the generalized thermal Janus core, Eq. (11) should be satisfied as well.

To experimentally demonstrate the validity of Figs. 5(b) and 5(c), one might also drill different holes in copper and lead plates to design practical structures of the core, and then design two samples; see Figs. 5(d)–5(f). Detailed parameters of the two samples are shown in Fig. 5(g). The simulated results based on the two samples are shown in Figs. 5(h) and 5(i), which agree well with our theoretical prediction as shown in Figs. 5(b) and 5(c).

In addition, when we rotate the core by 22.5°, 45°, and 67.5°, we can observe the switch progress from rotation to concentration: Figs. 6(a)–6(c) for anticlockwise rotation of the core and Figs. 6(d)–6(f) for clockwise rotation of the core. We also adjust the parameters h_1, h_2, w_1, and w_2 to observe the change in the rotation of heat flux; see Figs. 6(g)– 6(i). We mention that these parameters may affect κ_e according to Eqs. (7)–(9), but their influence is small enough to be neglected. The rotation degrees of heat flux in Figs. 6(a)–6(i) are about 26°, −20°, −18°, 55°, 38°, 18°, 68°, 60°, and 48°. The results show that the generalized thermal Janus core has a flexible control of heat flux rotation while keeping the external field undisturbed.

V. CONCLUSION

In summary, we have presented a theoretical framework to predict the effective thermal conductivity of a coated core with a heterogeneously architected core plus a homogeneous shell, which differs from the structure of a homogeneous core plus a heterogeneously architected shell as extensively adopted for thermal rotation and concentration according to the theory of transformation thermotics. Based on the theory, we have proposed two kinds of Janus structures, which enable flexible heat manipulation for thermal rotation and concentration. Our theory has been confirmed by numerical simulations and our design of Janus structures has been validated by both experiment and simulation. This work has not only potential applications in heat management, but also instructive meanings for exploring novel thermal phenomena of thermal metamaterials.

ACKNOWLEDGMENTS

We acknowledge the financial support by the National Natural Science Foundation of China under Grant No. 11725521, and by the Science and Technology Commission of Shanghai Municipality under Grant No. 16ZR1445100.

APPENDIX

Here we extend the theory from two dimensions (circular shape) to three dimensions (spherical shape). Then, the thermal property of the core can be represented by a heterogeneous, anisotropic, and diagonal thermal conductivity tensor $\overleftrightarrow{\kappa}_c(x, y, z)$,

$$\overleftrightarrow{\kappa}_c(x, y, z) = \begin{bmatrix} \kappa_{xx}(x, y, z) & 0 & 0 \\ 0 & \kappa_{yy}(x, y, z) & 0 \\ 0 & 0 & \kappa_{zz}(x, y, z) \end{bmatrix}. \tag{A1}$$

By imitating the two-dimensional results, Eqs. (7)–(9), we separate the core into sticks and calculate the effective thermal conductivity of each stick $\kappa_{xx}(y, z)$ through series connection pattern,

$$\kappa_{xx}(y, z) = \frac{2\sqrt{r_c^2 - y^2 - z^2}}{\int_{-\sqrt{r_c^2-y^2-z^2}}^{\sqrt{r_c^2-y^2-z^2}} \frac{dx}{\kappa_{xx}(x,y,z)}}, \tag{A2}$$

where r_c is the radius of the core.

We further calculate the effective thermal conductivity of these strips through a parallel connection pattern,

$$\kappa_c = \int_{-r_c}^{r_c} \frac{2\kappa_{xx}(y, z)\sqrt{r_c^2 - y^2 - z^2}\, dy\, dz}{(4/3)\pi r_c^3}. \tag{A3}$$

We finally calculate the effective thermal conductivity of the coated core κ_e through the single-particle effective medium theory, namely Eq. (11) in Ref. [30],

$$\kappa_e = \kappa_s \frac{\kappa_c + 2\kappa_s + 2(\kappa_c - \kappa_s)p}{\kappa_c + 2\kappa_s - (\kappa_c - \kappa_s)p}, \tag{A4}$$

where κ_s is the thermal conductivity of the shell, and $p = (r_c/r_s)^3$ is the volume fraction of the core.

[1] C. Z. Fan, Y. Gao, and J. P. Huang, Shaped graded materials with an apparent negative thermal conductivity, Appl. Phys. Lett. **92**, 251907 (2008).

[2] T. Y. Chen, C. N. Weng, and J. S. Chen, Cloak for curvilinearly anisotropic media in conduction, Appl. Phys. Lett. **93**, 114103 (2008).

[3] S. Guenneau, C. Amra, and D. Veynante, Transformation thermodynamics: Cloaking and concentrating heat flux, Opt. Express **20**, 8207 (2012).

[4] S. Narayana and Y. Sato, Heat Flux Manipulation with Engineered Thermal Materials, Phys. Rev. Lett. **108**, 214303 (2012).

[5] R. Schittny, M. Kadic, S. Guenneau, and M. Wegener, Experiments on Transformation Thermodynamics: Molding the Flow of Heat, Phys. Rev. Lett. **110**, 195901 (2013).

[6] H. Y. Xu, X. H. Shi, F. Gao, H. D. Sun, and B. L. Zhang, Ultrathin Three-Dimensional Thermal Cloak, Phys. Rev. Lett. **112**, 054301 (2014).

[7] T. C. Han, X. Bai, D. L. Gao, J. T. L. Thong, B. W. Li, and C. W. Qiu, Experimental Demonstration of a Bilayer Thermal Cloak, Phys. Rev. Lett. **112**, 054302 (2014).

[8] T. C. Han, X. Bai, J. T. L. Thong, B. W. Li, and C. W. Qiu, Full control and manipulation of heat signatures: Cloaking, camouflage and thermal metamaterials, Adv. Mater. **26**, 1731 (2014).

[9] T. Y. Chen, C. N. Weng, and Y. L. Tsai, Materials with constant anisotropic conductivity as a thermal cloak or concentrator, J. Appl. Phys. **117**, 054904 (2015).

[10] T. Z. Yang, Y. S. Su, W. K. Xu, and X. D. Yang, Transient thermal camouflage and heat signature control, Appl. Phys. Lett. **109**, 121905 (2016).

[11] R. Hu, S. L. Zhou, Y. Li, D. Y. Lei, X. B. Luo, and C. W. Qiu, Illusion thermotics, Adv. Mater. **30**, 1707237 (2018).

[12] S. L. Zhou, R. Hu, and X. B. Luo, Thermal illusion with twinborn-like heat signatures, Int. J. Heat Mass Transfer **127**, 607 (2018).

[13] R. Z. Wang, L. J. Xu, Q. Ji, and J. P. Huang, A thermal theory for unifying and designing transparency, concentrating and cloaking, J. Appl. Phys. **123**, 115117 (2018).

[14] L. J. Xu, R. Z. Wang, and J. P. Huang, Camouflage thermotics: A cavity without disturbing heat signatures outside, J. Appl. Phys. **123**, 245111 (2018).

[15] G. L. Dai, J. Shang, and J. P. Huang, Theory of transformation thermal convection for creeping flow in porous media: Cloaking, concentrating, and camouflage, Phys. Rev. E **97**, 022129 (2018).

[16] R. S. Kapadia and P. R. Bandaru, Heat flux concentration through polymeric thermal lenses, Appl. Phys. Lett. **105**, 233903 (2014).

[17] Y. Li, X. Y. Shen, J. P. Huang, and Y. S. Ni, Temperature-dependent transformation thermotics for unsteady states: Switchable concentrator for transient heat flow, Phys. Lett. A **380**, 1641 (2016).

[18] S. Guenneau and C. Amra, Anisotropic conductivity rotates heat fluxes in transient regimes, Opt. Express **21**, 6578 (2013).

[19] X. He and L. Z. Wu, Thermal transparency with the concept of neutral inclusion, Phys. Rev. E **88**, 033201 (2013).

[20] J. Y. Li, Y. Gao, and J. P. Huang, A bifunctional cloak using transformation media, J. Appl. Phys. **108**, 074504 (2010).

[21] Y. G. Ma, Y. C. Liu, M. Raza, Y. D. Wang, and S. L. He, Experimental Demonstration of a Multiphysics Cloak: Manipulating Heat Flux and Electric Current Simultaneously, Phys. Rev. Lett. **113**, 205501 (2014).

[22] M. Moccia, G. Castaldi, S. Savo, Y. Sato, and V. Galdi, Independent Manipulation of Heat and Electrical Current Via Bifunctional Metamaterials, Phys. Rev. X **4**, 021025 (2014).

[23] C. W. Lan, B. Li, and J. Zhou, Simultaneously concentrated electric and thermal fields using fan-shaped structure, Opt. Express **23**, 24475 (2015).

[24] T. Z. Yang, X. Bai, D. L. Gao, L. Z. Wu, B. W. Li, J. T. L. Thong, and C. W. Qiu, Invisible sensors: Simultaneous sensing

and camouflaging in multiphysical fields, Adv. Mater. **27**, 7752 (2015).

[25] X. Y. Shen, Y. Li, C. R. Jiang, Y. S. Ni, and J. P. Huang, Thermal cloak-concentrator, Appl. Phys. Lett. **109**, 031907 (2016).

[26] W. Z. Yang, Q. C. Liu, Z. Z. Gao, Z. F. Yue, and B. X. Xu, Theoretical search for heterogeneously architected 2D structures, Proc. Natl. Acad. Sci. U.S.A. **115**, E7245 (2018).

[27] K. Mitsumoto and H. Yoshino, Orientational ordering of closely packed Janus particles, Soft Matter **14**, 3919 (2018).

[28] W. J. Fei, M. M. Driscoll, P. M. Chaikin, and K. J. M. Bishop, Magneto-capillary dynamics of amphiphilic Janus particles at curved liquid interfaces, Soft Matter **14**, 4661 (2018).

[29] T. Debnath, Y. Y. Li, P. K. Ghosh, and F. Marchesoni, Hydrodynamic interaction of trapped active Janus particles in two dimensions, Phys. Rev. E **97**, 042602 (2018).

[30] S. Yang, L. J. Xu, R. Z. Wang, and J. P. Huang, Full control of heat transfer in single-particle structural materials, Appl. Phys. Lett. **111**, 121908 (2017).

[31] http://www.comsol.com/.

[32] L. J. Xu, C. R. Jiang, J. Shang, R. Z. Wang, and J. P. Huang, Periodic composites: Quasi-uniform heat conduction, Janus thermal illusion, and illusion thermal diodes, Eur. Phys. J. B **90**, 221 (2017).